

Differences between PAO and TA spectra: Systematics or indication of a local astrophysical source?

Pavlo Plotko,^{a,*} Arjen van Vliet,^{b,a} Xavier Rodrigues^{c,d,a} and Walter Winter^a

^aDeutsches Elektronen-Synchrotron DESY,
Platanenallee 6, 15738 Zeuthen, Germany

^aDepartment of Physics, Khalifa University,
P.O. Box 127788, Abu Dhabi, United Arab Emirates

^cEuropean Southern Observatory,
Karl-Schwarzschild-Straße 2, 85748 Garching bei München, Germany

^dAstronomical Institute, Fakultät für Physik und Astronomie, Ruhr-Universität Bochum,
44780 Bochum, Germany

E-mail: pavlo.plotko@desy.de

We present a joint fit of ultra-high-energy cosmic ray (UHECR) source scenarios to data from the Telescope Array (TA) and Pierre Auger Observatory (PAO) experiments [arXiv:2208.12274]. Our simulations account for the propagation of UHECRs through extragalactic space, considering a wide range of source parameters. We fit the spectrum and composition observed by both experiments, taking into account systematic errors. We compare three scenarios to explain the differences in the measured UHECR spectrum above 30 EeV. The first scenario is a systematic scenario with a cosmological homogeneous source distribution and an energy-dependent shift. The second scenario is an astrophysical scenario that combines a cosmological homogeneous source and a local source in the Northern Hemisphere with an energy-independent shift. The third scenario is a combined scenario that includes the presence of a local source, along with an energy-dependent systematic energy shift. Our results indicate that both the astrophysical and systematic scenarios explain the data equally well, while the combined scenario is too complex for the current data. All three scenarios provide similar results for parameters of the cosmological source distribution. We test different mass compositions emitted from the local source and conclude that the data are best described by a source lying at a distance below 26 Mpc that emits cosmic rays dominated by the silicon mass group. In the best-fit astrophysical scenario, the local source lies at a distance of 15 Mpc and emits cosmic rays dominated by the silicon mass group. We discuss other possible parameter combinations and potential source candidates by comparing these results with recent TA anisotropy measurements.

38th International Cosmic Ray Conference (ICRC2023)
26 July - 3 August, 2023
Nagoya, Japan



*Speaker

1. Introduction

Ultra-high-energy cosmic rays (UHECRs), atomic nuclei with energies above 10^{18} eV, are the most energetic particles detected to date. Their detection and analysis are facilitated by two primary observatories: the Pierre Auger Observatory [henceforth PAO, 1] in Argentina and the Telescope Array [TA, 2, 3] in Utah, USA. These observatories employ a hybrid detection technique to detect the extensive air showers in the atmosphere instigated by UHECRs, utilizing a surface detector array to measure charged secondaries reaching ground level and fluorescence detector stations to monitor the development of the air showers in the atmosphere.

Geographical positioning dictates that PAO and TA observe distinct portions of the sky, with PAO monitoring the Southern Hemisphere with declination below 24.8° [4] and TA observing the Northern Hemisphere with declination above -16.0° . However, a common declination band, $-16.0^\circ < \delta < 24.8^\circ$ [5], can be observed by both observatories, offering an opportunity for joint analysis.

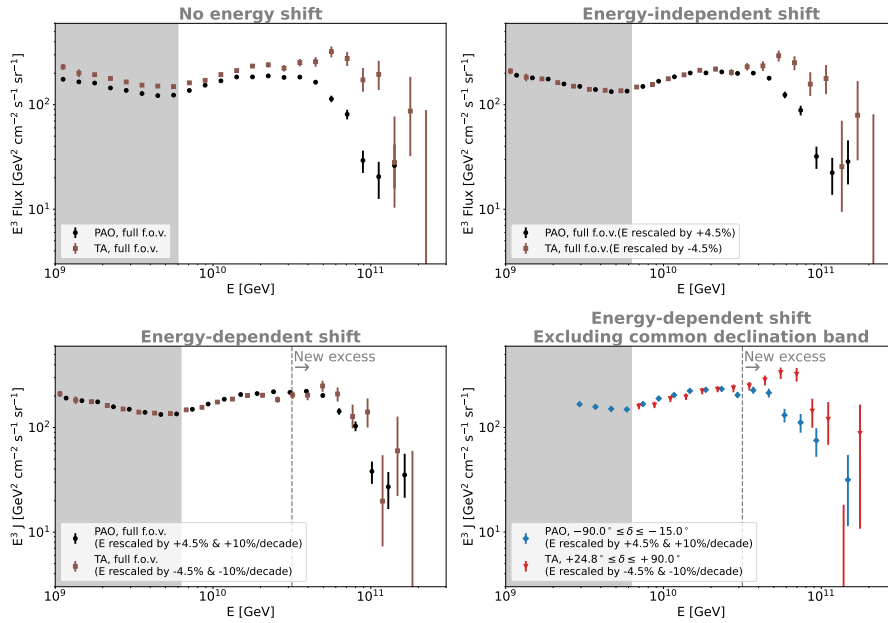


Figure 1 The black circles and brown squares points represent the energy spectrum of the UHECRs as measured by PAO and TA in the full fields of view (f.o.v.) of either observatory. In the upper left plot we see the data in the native energy scale of either experiment; in the upper right plot, those energy scales have been shifted by $\pm 4.5\%$. In the bottom left plot, the data are shifted by an energy-dependent shift (see [8]). In the bottom right plot, the same energy-dependent shift is applied to the PAO spectrum from the Southern Hemisphere (blue diamonds) and the TA spectrum from the Northern Hemisphere (red triangles). Data adopted from the analyses by [7, 8].

Recent collaborative work between PAO and TA has identified discrepancies in the energy spectrum of UHECRs at energies above $10^{19.5}$ eV, or about 30 EeV [6–8], as shown in the upper left plot of Fig. 1. These discrepancies persist even when considering only the common declination

band, albeit less significantly due to higher statistical uncertainties. The total systematic uncertainty in the energy scale of PAO is estimated at 14% [4], while for TA it is 21% [5].

To address these discrepancies, it becomes necessary to implement shifts in the energy scales of both experiments. These shifts can be categorized into two types: energy-independent and energy-dependent [8]. The energy-independent shift is a constant value applied across the entire energy scale. This shift mitigates the spectral differences below 30 EeV, as we can see in the upper right plot of Fig. 1. However, above that energy, the spectra become again discrepant, with TA data showing an excess in flux compared to PAO. The energy-dependent shift varies with the energy value, which is need to explain discrepancy in the spectrum at energy above 30 EeV. Despite the application of these shifts, residual differences are observed when data from the common declination band is excluded, as shown in the left bottom plot of Fig. 1. This observation implies that the systematic uncertainties of the experiments could be dependent on declination, or that the observed effect might have an astrophysical origin, or both.

Previous analyses of TA support the existence of a nearby UHECR source or group of sources [9–11]. Several astrophysical models predict that nearby sources could describe the PAO spectrum at the highest energies [12–15].

In this work, we test the systematic and astrophysical hypotheses for the discrepancy between the PAO and TA spectrum.

2. Method

We simulate UHECR emission from a cosmological population of sources, assumed to be homogeneously distributed. The emission spectrum of each element A from the cosmological source distribution, J_A^{cosmo} , is parameterized as:

$$J_A^{\text{cosmo}}(E, z) = J_0^{\text{cosmo}} f_A n(z, m_{\text{cosmo}}) \left(\frac{E}{10^9 \text{ GeV}} \right)^{-\gamma_{\text{cosmo}}} f_{\text{cut}}(E, R_{\text{cosmo}}^{\text{max}}), \quad (1)$$

where $n = (1+z)^{m_{\text{cosmo}}}$ is the cosmological source density, γ_{cosmo} is the spectral index of the emitted cosmic rays, J_0^{cosmo} is the normalization of the spectra, and f_{cut} introduces an exponential cutoff at the energy corresponding to the maximum rigidity $R_{\text{cosmo}}^{\text{max}} = E_{\text{max}}/Z_A$.

We assume that the local source emits a single mass group from the five listed above. Therefore, the emission from this source can be fully characterized by a maximum rigidity $R_{\text{local}}^{\text{max}}$, power-law index γ_{local} , emission luminosity $L_{\text{local}}^{\text{CR}}$, the comoving distance D_{local} , and one emitted cosmic-ray mass group. We then propagate UHECRs from their sources to Earth in 1D using PRINCE [16]. Additionally, we consider 3 air shower models: SIBYLL 2.3c [21], EPOS-LHC [22], and QGSJET-II-04 [23]. While we primarily discuss results for SIBYLL 2.3c, results for other air shower models can be found in [?]

Our aim is to describe the spectrum and composition ($\langle X_{\text{max}} \rangle$ and $\sigma(X_{\text{max}})$) of UHECRs above $E_{\text{min}} = 6 \times 10^9$ GeV, originating from the entire field of view of TA and PAO. Additionally, we incorporate spectrum data from either observatory at energies lower than 6×10^9 GeV into our analysis, treating these as upper limits.

The goodness of a fit relative to the PAO and TA data is calculated by means of a χ^2 test. We then compute the goodness of the joint fit, combining the χ^2 values from both experiments with the systematic uncertainties.

A simultaneous scan of all parameters would be computationally expensive, so instead we divide it into two steps. First, we perform a scan assuming only a cosmological source distribution. We consider the spectral and composition data from PAO in our entire energy range, as well as TA data below 25 EeV. We then fit the TA data in the full energy range, assuming the experiment observes (1) the cosmological source distribution, with the parameter previously obtained, and (2) a local source, which parameters we now optimize. This two-step approach does not affect the results because above 30 EeV, where the experiments differ, the overall fit is driven mainly by the PAO spectrum (due to its lower uncertainties), and therefore depends primarily on the cosmological source distribution.

We test three different scenarios: A) both TA and PAO observe the same cosmological source distribution and an energy-dependent shift; B) the assumption that TA additionally observes a local source in the Northern Hemisphere, along with an energy-independent shift; C) the presence of a local source in the Northern Hemisphere observed by TA, along with an energy-dependent shift. To evaluate our hypothesis, we use the Akaike Information Criterion with correction (AICc) [17]. The model with the smallest AICc provides the best fit to the data.

3. Results and Discussion

The astrophysical scenario is favored over the systematic scenario at the 0.8σ level, indicating that both scenarios could explain the data equally well. However, it's important to note that the combined scenario provides a poorer fit and is excluded at the 2.0σ level compared to the systematic scenario. Despite having a lower χ^2 value, this scenario requires the inclusion of four additional parameters for a local source.

In Fig. 2 we show the best-fit results for all three scenarios, obtained using SIBYLL2.3c as the air shower model. The best-fit spectrum for the cosmological source distribution is similar in all cases. For the astrophysical scenario, the best fit is dominated by nitrogen at the 75-85% level, followed by silicon. The proton component is absent for the best-fit scenario, and the protons in the propagated spectrum at Earth are therefore only secondaries. For both the systematic and combined scenarios, helium, nitrogen, and silicon are present at comparable levels. The contribution from the local source is almost entirely composed of the same mass group originally emitted by the source, as indicated by the solid yellow curve for the astrophysical scenario and the solid blue curve for the combined scenario. This is due to the relative proximity of the source.

Fig. 3 illustrates the parameter space of the cosmological source distribution for all scenarios. The white dots represent the best-fit parameters, which correspond to the results of Fig. 2. Notably, the 1σ region is similar for all three models and predicts a negative source evolution and a soft spectral index for the cosmological source distribution for all three scenarios. In contrast, the 1σ results from [16] indicate a positive source evolution and a harder spectral index. The differences between our results and those of [16] are primarily due to our inclusion of upper limits on the spectrum at energies lower than $E_{\min} = 6 \times 10^9$ GeV. These constraints mainly affect the flux of

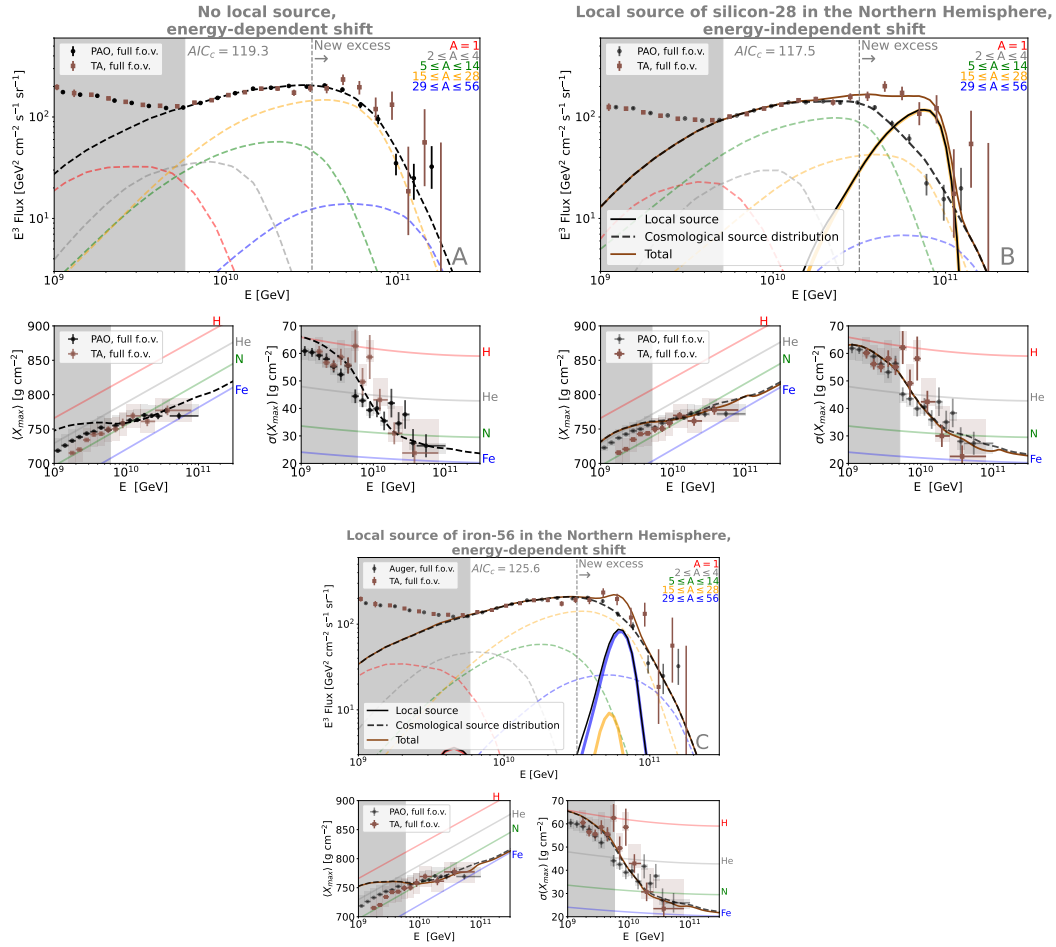


Figure 2 Spectra (upper plot in each panel) and composition observables (two lower plots in each panel) resulting from a joint fit to TA and PAO data, using SIBYLL 2.3c as the air shower model. The upper plot and the lower plots in each panel show the predicted cosmic-ray spectra and composition, respectively. The dashed black curves represent the contribution of the cosmological source distribution, which is observed by both experiments. The contributions from different mass groups are shown in different colors. The brown curves represent the sum of the cosmological source distribution and the local source, which is the total flux observed by TA. The upper left panel shows the best fit considering the energy-dependent shift without a local source. In the upper right panel, we show a scenario of the energy-independent shift with the additional presence of a local source of silicon-28. The bottom plots show the best fit, considering the energy-dependent shift with the additional presence of a local source of iron-56.

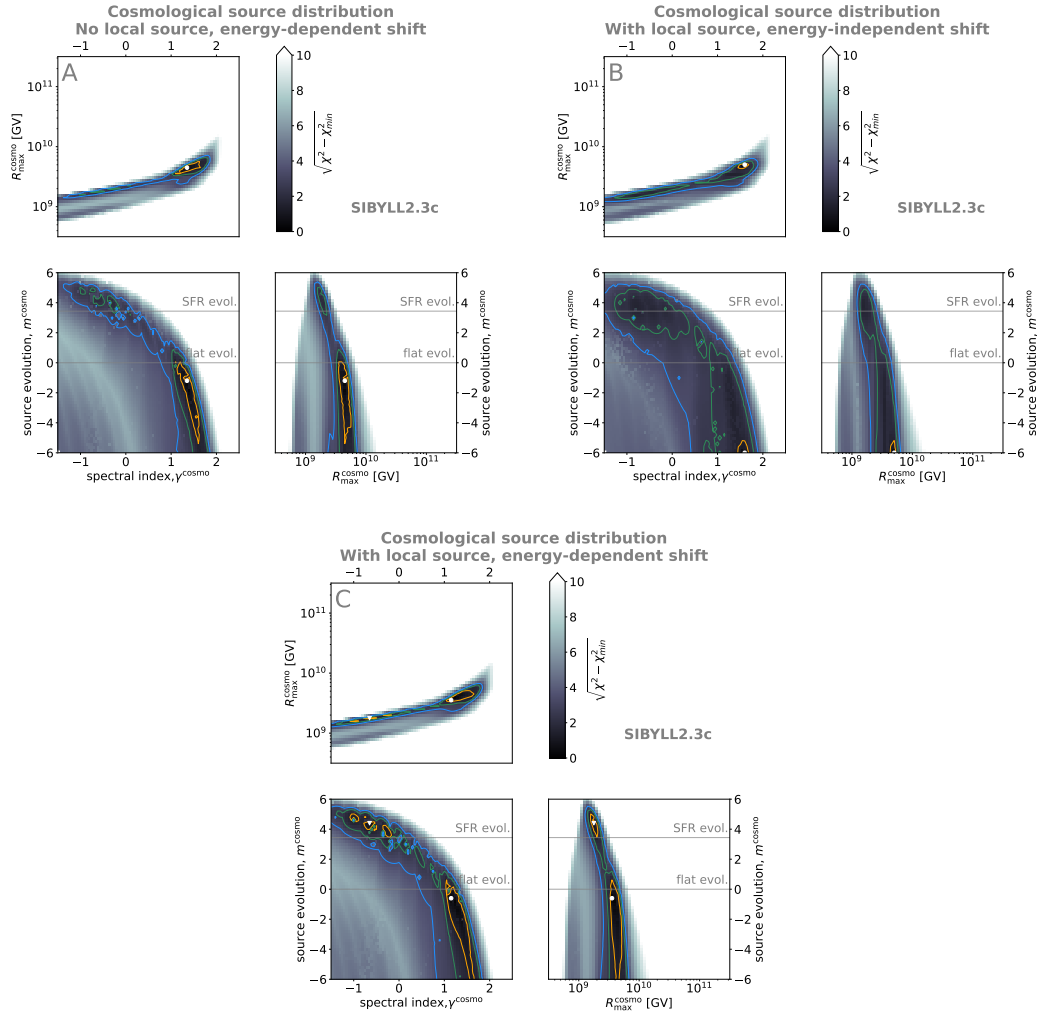


Figure 3 Parameter space of a cosmological source distribution based on a joint fit to TA and PAO data. In the upper left panel, we assume an energy-dependent shift with no local source. In the upper right panel, we assume an energy-independent shift with a local source in the Northern Hemisphere. In the bottom panel, we assume the energy-dependent shift with a local source in the Northern Hemisphere. The white dots in each plot correspond to the best-fit parameters of each scenario. In the case of an energy-dependent shift with a local source, there is a second minimum, marked as a white triangle. The colored shading corresponds to the χ^2 value compared to the best fit, while the yellow, green and blue contours indicate the 1-, 2- and 3σ regions, respectively, calculated for two d.o.f. In each panel, the parameter that is not shown is treated as a nuisance parameter and minimized over.

secondary protons from disintegration. In the case of an energy-dependent shift with a local source, there is a second minimum which is similar to the 1σ region from [16].

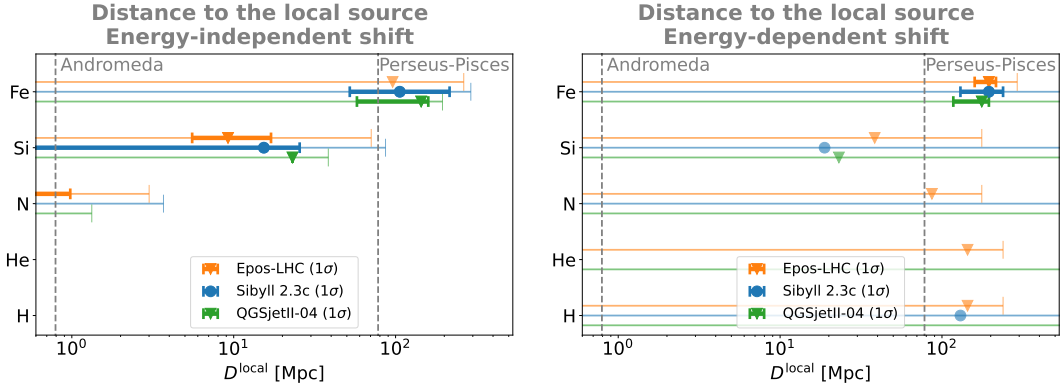


Figure 4 Best-fit results on the travel distance of the cosmic rays emitted by the local source for the energy-independent shift, depending on the emitted isotope, in the 1σ region (bold error bars) and 3σ (thin error bars), for one degree of freedom. The colors refer to the three different air shower models.

Finally, the distance to the local source is also constrained. The best fit was found for silicon-28 and iron-56 at distances of 13.9 Mpc and 195 Mpc for the case of an energy-independent and energy-dependent shift, respectively. We show in the left and right plots of Fig. 4 the 1σ and 3σ uncertainty regions on the distance traveled by the cosmic rays from the local source to Earth, for five different emitted isotopes, for energy-independent and energy-dependent shift, respectively. For comparison, we show Andromeda (M31), which lies at a distance of 752 ± 27 kpc [24] and within the contour region of the new excess of TA. Our neighboring galaxy is therefore a potential local UHECR source candidate for intermediate-mass isotopes like nitrogen and silicon. On the other hand, a source such as the Perseus-Pisces supercluster (PPS, also known as A 426), at 70 Mpc, would satisfy the distance criterion for isotopes in the iron group. Both these objects are also supported as possible local source candidates by current data from TA, since their position is compatible with the direction of the high-energy excess recently detected [25]

Follow-up, more detailed analyses require 1) a better understanding of possible energy-dependent systematics, 2) the inclusion of different detector acceptances and resolutions, as well as the differences between the analysis techniques of the PAO and for the composition data, 3) an unambiguous association with (possibly observed) anisotropies 4) performing a joint fit for different declination bands. On the modeling side, we have restricted ourselves to a single mass group from the local source due to the computational effort. However, a more complex model involving a mix of isotopes may eventually provide a better joint fit and could further constrain the properties of the local source. However, the higher number of parameters of such a model will require higher statistics from the Northern Hemisphere, which can only be made possible by future experiments such as the planned TAx4 experiment [26]

References

- [1] Aab, A., et al. 2015, Nucl. Instrum. Meth. A, 798, 172,

- [2] Abu-Zayyad, T., et al. 2013, Nucl. Instrum. Meth. A, 689, 87,
- [3] Tokuno, H., et al. 2012, Nucl. Instrum. Meth. A, 676, 54,
- [4] Aab, A., Abreu, P., Aglietta, M., et al.. 2020, Phys. Rev. D, 102, 062005,
- [5] Ivanov, D 2019, PoS, ICRC2019, 298,
- [6] Ivanov, D. 2017, PoS, ICRC2017, 498,
- [7] Deligny, O. 2019, PoS, ICRC2019, 234,
- [8] Tsunesada, Y., Abbasi, R., Abu-Zayyad, T., et al. 2021, PoS, ICRC2021, 337,
- [9] Abbasi, R. U., Abe, M., Abu-Zayyad, T., et al. 2014, The Astrophysical Journal, 790, L21,
- [10] Globus, N., Allard, D., Parizot, E., Lachaud, C., & Piran, T. 2017, Astrophys. J., 836, 163,
- [11] Abbasi, R. U., Abu-Zayyad, T., Allen, M., et al. 2021, Indications of a Cosmic Ray Source in the Perseus-Pisces Supercluster,
- [12] Wibig, T., & Wolfendale, A. W. 2007,
- [13] Taylor, A. M., Ahlers, M., & Aharonian, F. A. 2011, Phys. Rev. D, 84, 105007,
- [14] Mollerach, S., & Roulet, E. 2019, Phys. Rev. D, 99, 103010,
- [15] Lang, R. G., Taylor, A. M., Ahlers, M., & de Souza, V. 2020, Phys. Rev. D, 102, 063012,
- [16] Heinze, J., Fedynitch, A., Boncioli, D., & Winter, W. 2019, The Astrophysical Journal, 873, 88
- [17] Akaike, H. 1974, IEEE Transactions on Automatic Control, 19, 716,
- [18] de Souza, V. 2017, PoS, ICRC2017, 522,
- [19] Koning, A. J., Hilaire, S., & Duijvestijn, M. C. 2007, in Proceedings, International Conference on Nuclear Data for Science and Tecnology, 211–214
- [20] Gilmore, R. C., Somerville, R. S., Primack, J. R., & Domínguez, A. 2012, Monthly Notices of the Royal Astronomical Society, 422, 3189,
- [21] Riehn, F., Engel, R., Fedynitch, A., Gaisser, T., & Stanev, T. 2016, PoS, ICRC2015, 558,
- [22] Pierog, T., Karpenko, I., Katzy, J. M., Yatsenko, E., & Werner, K. 2015, Phys. Rev. C, 92, 034906,
- [23] Ostapchenko, S. 2011, Phys. Rev. D, 83, 014018,
- [24] Riess, A. G., Fliri, J., & Valls-Gabaud, D. 2012, The Astrophysical Journal, 745, 156
- [25] Kim, J., Ivanov, D., Kawata, K., Sagawa, H., & Thomson, G. 2021, PoS, ICRC2021, 328
- [26] Abbasi, R. U., et al. 2021, PoS, ICRC2021, 355